

A suppressed contribution of low mass galaxies to reionization due to supernova feedback

J. Stuart B. Wyithe¹, Abraham Loeb²

¹ *School of Physics, University of Melbourne, Parkville, Victoria, Australia*

² *Astronomy Department, Harvard University, 60 Garden Street, Cambridge, MA 02138, USA*

Email: swyithe@unimelb.edu.au; aloeb@cfa.harvard.edu

19 October 2018

ABSTRACT

Motivated by recent observations of the star formation rate density function out to $z \sim 7$, we describe a simple model for the star formation rate density function at high redshift based on the extended Press-Schechter formalism. This model postulates a starburst following each major merger, lasting for a time t_{SF} and converting at most $f_{\star, \text{max}}$ of galactic gas into stars. We include a simple physical prescription for supernovae feedback that suppresses star formation in low mass galaxies. Constraining t_{SF} and $f_{\star, \text{max}}$ to describe the observed star formation rate density at high redshifts, we find that individual starbursts were terminated after a time $t_{\text{SF}} \sim 10^7$ years. This is comparable to the main-sequence lifetimes of supernova progenitors, indicating that high redshift starbursts are quenched once supernovae feedback had time to develop. High redshift galaxies convert $\sim 10\%$ of their mass into stars for galaxies with star formation rates above $\sim 1M_{\odot} \text{ yr}^{-1}$, but a smaller fraction for lower luminosity galaxies. Our best fit model successfully predicts the observed relation between star formation rate and stellar mass at $z \gtrsim 4$, while our deduced relation between stellar mass and halo mass is also consistent with data on the dwarf satellites of the Milky Way. We find that supernovae feedback lowers the efficiency of star formation in the lowest mass galaxies and makes their contribution to reionization small. As a result, photoionization feedback on low mass galaxy formation does not significantly affect the reionization history. Using a semi-analytic model for the reionization history, we infer that approximately half of the ionizing photons needed to complete reionization have already been observed in star-forming galaxies.

Key words: galaxies: formation, high-redshift, — cosmology: theory, diffuse radiation

1 INTRODUCTION

The galaxy luminosity function is the primary observable that must be reproduced by any successful model of galaxy formation. At $z \gtrsim 6$, it also represents one of the most important observables for studying the reionization of cosmic hydrogen. Developing a theoretical picture of the important processes involved in setting the star formation rate at high redshift lies at the forefront of understanding this important cosmic epoch (e.g. Trenti et al. 2010; Finlator et al. 2011; Muñoz & Loeb 2011; Raičević et al. 2011; Salvaterra et al. 2011).

The luminosity function of Lyman-break galaxy candidates discovered at $z \gtrsim 6$ in the Hubble Ultra-Deep Field is described by a Schechter function with characteristic density Ψ_{\star} in comoving Mpc^{-3} , and a power-law slope α at luminosities L below a characteristic break L_{\star} (e.g. Bouwens

et al. 2011). Observations show that the value of L_{\star} decreases towards higher redshift as expected from the dark matter halo mass-function (e.g. Muñoz & Loeb 2011), while the faint end slope of $\alpha \approx -1.8$ is observed to be roughly independent of redshift (McLure et al. 2009; Bouwens et al. 2011). A complication that arises when modelling the luminosity function is that models predict a star formation rate, which must then be converted to a luminosity assuming an initial mass function (IMF) for the stars. While this calculation is straightforward, of more importance is the potential contribution of reddening. As shown by Bouwens et al. (2012), the blue continuum slope of $z \gtrsim 6$ galaxies is dependent on luminosity and redshift. As a result there is a dust correction which is both luminosity and redshift dependent and difficult to reproduce from first principles reliably in a simple model. This renders theoretical studies of the luminosity function difficult to interpret. For exam-

ple, in the model of Muñoz & Loeb (2011) a distribution of mass-to-light ratios is assumed whose mean is independent of mass, while in Trenti et al. (2010) the mass-to-light ratio is assumed to be independent of redshift. Neither of these assumptions holds based on the more recent observational work of Bouwens et al. (2012). More complex models are able to better reproduce many of the observed properties, and so make more robust predictions of the physics. For example Finlator et al. (2011) have modelled the growth of stellar mass in high redshift galaxies using hydrodynamical simulations coupled with sub-grid models for processes including star formation and metal enrichment, and broadly reproduce the luminosity function evolution as well as the blue colours of the young stellar populations at high redshift. Similarly, Salvaterra et al. (2011) and Jaacks et al. (2012) have calculated the evolution of the luminosity function in detailed numerical simulations including calculations of enrichment and dust reddening, with the latter also including additional physics related to the transition from population-III to population-II stars. A focus of these numerical studies is the role of supernova (SNe) feedback on star formation, particularly in low mass systems. In a separate approach, Raičević et al. (2011) (see also Benson et al. 2006; Lacey et al. 2011) used a semi-analytical galaxy formation code based on Monte-Carlo merger trees to model the evolution of the high redshift luminosity function, and study the effect of SNe feedback on the global ionizing photon budget and global ionization. In particular Raičević et al. (2011) evaluated the ionizing photon budget, finding that although galaxies should produce sufficient ionizing photons to complete reionization, most of the galaxies responsible would be below the detection threshold of current surveys.

A simpler way to constrain theory by observations is to estimate the star formation rate density observationally, where the correction is made from luminosity to star formation rate using the observed continuum properties of the galaxies under study. A powerful probe of the physics of star formation is then provided by the star formation rate density function (i.e. the number of galaxies per unit volume per unit star formation rate). Recently, this has become a viable approach following the work of Smit et al. (2012) who combined estimates of dust extinction at $z \sim 4-7$ with measurements of the UV luminosity function in order to derive star formation rate density (SFRD) functions at $z \sim 4, 5, 6$ and 7 . These SFRD functions provide a physical description of the build-up of stellar mass in galaxies at high redshift. The resulting SFRD functions are well-described by a Schechter function, with a characteristic break separating a shallow dependence of SFRD on star formation rate at low luminosities from the exponential dependence at high luminosities. As mentioned, the physics of star formation in high redshift galaxies has important implications for the process of reionization. Of particular interest is the star formation rate in low mass systems. For example, it has been shown that the growth of HII regions during reionization may be influenced by radiative feedback in the form of suppression of galaxy formation below the cosmological Jeans mass within a heated intergalactic medium (IGM) (Dijkstra et al. 2004), although the importance of this effect remains controversial (Mesinger & Dijkstra 2008). If present, this radiative suppression of low mass galaxy-formation delays and extends the reionization process, which though started by low

mass galaxies, must then be completed by relatively massive galaxies (e.g. Iliev et al. 2007). On the other hand, the semi-analytic modelling of Raičević et al. (2011) indicates that photoionization suppression of star formation in these low mass galaxies is unlikely to significantly affect reionization, because of feedback effects on the star formation efficiency implies that their contribution to reionization is small. The contribution of galaxies to the reionization of the IGM is dependent on the star formation rate and initial stellar mass function, but is also limited by the fraction of ionizing photons that escape their host galaxies. If the escape fraction is small, then star formation had to be very efficient at high redshift in order to reionize the Universe. The escape fraction is therefore a critical parameter in studies of the connection between high redshift galaxy formation and reionization. Attempts to determine the escape fraction have been dominated by direct observations of relatively low redshift galaxies, and by numerical simulation. Both observational (e.g. Steidel et al. 2001; Fernández-Soto et al. 2003; Shapley et al. 2006; Siana et al. 2007), and theoretical (e.g. Razoumov & Sommer-Larsen 2006; Yajima et al. 2009; Gnedin et al. 2007; Wise & Cen 2009) estimates of the escape fraction at the Lyman-limit are currently uncertain, with an expected range of $0.01 \lesssim f_{\text{esc}} \lesssim 1$.

In this paper we aim to utilise this new determination of the build up of stellar mass at high redshift to constrain star formation scenarios in high redshift galaxies, with particular attention to the possible consequences of SNe feedback for the reionization of hydrogen. In § 2, we describe an analytic model for the star formation rate density function at high redshift based on the extended Press-Schechter formalism (Lacey & Cole 1993) with a simple physical prescription for SNe feedback that suppresses star formation in low mass galaxies. We confront our model with the observed SFRD function in § 3 in order to constrain the starburst lifetime and the stellar mass – star formation rate relation, and show the predictions of the model for the escape of ionizing photons from star-forming galaxies in § 4. We investigate the implications for the reionization history in § 5-6, and conclude in § 7. In our numerical examples, we adopt the standard set of cosmological parameters (Komatsu et al. 2011), with values of $\Omega_b = 0.04$, $\Omega_m = 0.24$ and $\Omega_\Lambda = 0.76$ for the density parameters of matter, baryon, and dark energy, respectively, $h = 0.73$, for the dimensionless Hubble constant, and $\sigma_8 = 0.82$.

2 MODEL

The star formation rate in a galaxy halo of mass M that turns a fraction f_* of its disk mass $m_d M$ into stars over a time t_{SF} is

$$SFR = 0.15 M_\odot \text{yr}^{-1} \left(\frac{m_d}{0.17} \right) \left(\frac{f_*}{0.1} \right) \left(\frac{M}{10^8 M_\odot} \right) \left(\frac{t_{\text{SF}}}{10^7 \text{yr}} \right)^{-1}. \quad (1)$$

We assume that major mergers trigger bursts of star formation, and constrain the starburst lifetime required to reproduce the observed star formation rate density function. The star formation rate density function (i.e. galaxies per Mpc^{-3}

per unit of SFR) can be estimated as

$$\Phi(SFR) = \epsilon_{\text{duty}} \left(\Delta M t_{\text{H}} \frac{dN_{\text{merge}}^2}{dt d\Delta M} \Big|_{M_1, \Delta M} \frac{dn}{dM} \right) \left(\frac{dSFR}{dM} \right)^{-1}, \quad (2)$$

where ϵ_{duty} is the fraction of the Hubble time (t_{H}) over which each burst lasts, and dn/dM is mass function of dark matter halos (Press & Schechter 1974; Sheth & Tormen 1999). The rate of major mergers (dN_{merge}/dt) is calculated as the number of halos per logarithm of mass ΔM per unit time that merge¹ with a halo of mass M_1 to form a halo of mass M (Lacey & Cole 1993). We assign a 2:1 mass ratio to major mergers (i.e. $M_1 = \frac{2}{3}M$ and $\Delta M = M/3$). The ionizing photon rate from a starburst drops rapidly once the most massive stars fade away on a timescale of $t_s \sim 3 \times 10^6$ years (Barkana & Loeb 2001). If the starburst lifetime t_{SF} is much longer than t_s , then the duty cycle associated with a starburst is set by t_{SF} . However, if the starburst is shorter than t_s , the star formation remains visible for a minimum of t_s . Thus the duty-cycle is

$$\epsilon_{\text{duty}} = \frac{t_s + t_{\text{SF}}}{t_{\text{H}}}. \quad (3)$$

For comparison with observations we define

$$\Psi(SFR) = \ln 10 \times SFR \times \Phi, \quad (4)$$

which has units of Mpc^{-3} per dex.

We expect that SNe feedback will alter the fraction of gas in a galaxy that is turned into stars (e.g. Dekel & Woo 2003). To determine the mass and redshift dependence of f_* in the presence of SNe we suppose that stars form with an efficiency f_* out of the gas that collapses and cools within a dark matter halo and that a fraction F_{SN} of each supernova energy output, E_{SN} , heats the galactic gas mechanically (allowing for some losses due to cooling). The mechanical feedback will halt the star formation once the cumulative energy returned to the gas by supernovae equals the total thermal energy of gas at the virial velocity of the halo (e.g. Wyithe & Loeb 2003b). Hence, the limiting stellar mass is set by the condition

$$\frac{M_*}{w_{\text{SN}}} E_{\text{SN}} F_{\text{SN}} f_t f_d = E_b = \frac{1}{2} m_d M v_{\text{vir}}^2. \quad (5)$$

In this relation E_b is the binding energy in the halo, w_{SN} is the mass in stars per supernova explosion, and the total stellar mass is $M_* = m_d M f_{*,\text{tot}}$ where $f_{*,\text{tot}} = N_{\text{merge}} f_*$ is the total fraction of the gas that is converted to stars during major mergers, and N_{merge} is the number of major mergers per Hubble time. The parameters f_t and f_d denote the fraction of the SNe energy that contributes because of the finite timescale of the SNe feedback or the disk scale height being smaller than the SNe bubble. These terms are described in more detail below.

The ratio between the total mass in stars and dark matter is observed to increase with halo mass as $(M_*/M) \propto$

$M^{0.5}$ for $M_* \lesssim 3 \times 10^{10} M_{\odot}$, but is constant for larger stellar masses (Kauffmann et al. 2003). Thus, the star formation efficiency within dwarf galaxies decreases towards low masses. For comparison with equation (5), a Scalo (1998) mass function of stars has $w_{\text{SN}} \sim 126 M_{\odot}$ per supernova and $E_{\text{SN}} = 10^{51}$ ergs, and so we find that $M_* = 3 \times 10^{10} M_{\odot}$ and $v_c \sim 175$ km/s (the typical value observed locally; see e.g. Bell & de Jong 2001) implies $f_{*,\text{tot}} \sim 0.1$ for a value of $F_{\text{SN}} \sim 0.5$. Smaller galaxies have smaller values of f_* . Equation (5) indicates that

$$f_* = \min \left[f_{*,\text{max}}, \frac{0.008}{N_{\text{merge}}} \left(\frac{M}{10^{10} M_{\odot}} \right)^{\frac{2}{3}} \left(\frac{1+z}{10} \right) (f_t f_d F_{\text{SN}})^{-1} \right] \quad (6)$$

We utilise equation (6) with equation (2) as a function of the parameters t_{SF} and $f_{*,\text{max}}$.

2.1 Disk structure

The effect of SNe feedback is dependent on the conditions of the interstellar medium (ISM) gas. We assume that the cold gas (out of which stars form) occupies a self-gravitating exponential disk, with surface mass density $\Sigma(r) = \Sigma_0 e^{-r/R_d}$, where

$$\Sigma_0 = \frac{m_d M}{2\pi R_d^2}, \quad (7)$$

and R_d is the scale radius

$$R_d = \frac{\lambda}{\sqrt{2}} R_{\text{vir}}, \quad (8)$$

where m_d is the mass fraction of the disk relative to the halo and $\lambda \sim 0.05$ is the spin parameter of the halo (Mo et al. 1998). The virial radius of a halo with mass M_{halo} is given by the expression

$$R_{\text{vir}} = 0.784 h^{-1} \text{ kpc} \left(\frac{M_{\text{halo}}}{10^8 M_{\odot}} \right)^{\frac{1}{3}} [\zeta(z)]^{-\frac{1}{3}} \left(\frac{1+z}{10} \right)^{-1},$$

where $\zeta \equiv [(\Omega_m/\Omega_m^z)(\Delta_c/18\pi^2)]$, $\Omega_m^z \equiv [1 + (\Omega_{\Lambda}/\Omega_m)(1+z)^{-3}]^{-1}$, $\Delta_c = 18\pi^2 + 82d - 39d^2$, and $d = \Omega_m^z - 1$ (see equations 22–25 in Barkana & Loeb 2001, for more details). The scale height of the disk at radius r is

$$H = \frac{c_s^2}{\pi G \Sigma(r)}. \quad (9)$$

We adopt the density in the mid plane at the scale radius, within which half the gas is contained, as representative of the density of the ISM. At $r = R_d$ the scale height is

$$\begin{aligned} H &= \frac{2c_s^2 R_d^2 \times 2.71}{G m_d M} \\ &= 0.034 \text{ kpc} \left(\frac{\lambda}{0.05} \right)^2 \left(\frac{m_d}{0.17} \right)^{-1} \left(\frac{M}{10^8 M_{\odot}} \right)^{-1/3} \\ &\quad \times \left(\frac{1+z}{10} \right)^{-2} \left(\frac{c_s}{10 \text{ km/s}} \right)^2. \end{aligned} \quad (10)$$

The number density of particles in the mid plane at $r = R_d$ is

$$n_p = \frac{G(m_d M)^2}{8\pi m_p c_s^2 R_d^4 \times 2.71^2}, \quad (11)$$

where m_p is the mass density of particles.

¹ In addition to the excursion set approach of (Lacey & Cole 1993), we have also computed merger rates using the fitting formulae based on numerical simulations of Fakhouri et al. (2010). We find consistent results using either approach.

We note that if the gas disk becomes stable to fragmentation at a radius beyond which there is a significant fraction of gas by mass, then the half mass radius of the stellar disk may not equal the scale radius of the gas-disk. However, Wyithe & Loeb (2011) find that the disk becomes stable (based on Toomre- Q criterion) only at 3–4 scale radii.

2.2 Supernova evacuation of the ISM

Clarke & Oey (2002) presented a simple analytic model for the effect of supernovae on the interstellar medium which we apply to high redshift galaxies. In this model, clusters of N_e SNe produce super-bubbles in the ISM with a radius R_e at which the super-bubble comes into pressure balance with the ISM. This radius can be found by approximating R_e as the radius within which the thermal energy of the ISM equals the mechanical energy of the SNe cluster. The timescale associated with the evacuation of a super bubble in the ISM by a SNe cluster is $t_e = 4 \times 10^7$ years, corresponding to the lifetime of the lowest mass SNe progenitor. The evacuation radius for a cluster of N_e SNe, each with energy output E_{SN} within an ISM of sound speed c_s is therefore

$$R_e = \left(\frac{2N_e E_{\text{SN}}}{2\pi m_p n_p c_s^2} \right)^{\frac{1}{3}}, \quad (12)$$

yielding

$$R_e = 0.08 \text{ kpc} \left(\frac{N_e}{10} \right)^{\frac{1}{3}} \left(\frac{E_{\text{SN}}}{10^{51} \text{ erg}} \right)^{\frac{1}{3}} \left(\frac{\lambda}{0.05} \right)^{\frac{4}{3}} \left(\frac{m_d}{0.17} \right)^{-\frac{2}{3}} \times \left(\frac{M}{10^8 M_\odot} \right)^{-\frac{2}{3}} \left(\frac{1+z}{10} \right)^{-\frac{4}{3}}. \quad (13)$$

The derived value of R_e ignores radiative losses of the super-bubble before it comes into pressure equilibrium with the ISM. Clarke & Oey (2002) evaluated the validity of this assumption by noting that in galaxies like the Milky-Way, the radius at which cooling becomes important is larger than the radius at which the super-bubble comes into pressure equilibrium. Of importance here is the clustering of SNe, which concentrates the mechanical output into small regions of the ISM. At high redshift, cooling is expected to be more efficient in the much denser ISM, although this will be offset by the lower gas metallicity. Mac Low & McCray (1988) derived the cooling radius to be

$$R_c = 350 \text{ pc} \left(\frac{L}{10^{38} \text{ erg/s}} \right)^{4/11} n_p^{-7/11} \zeta^{-27/22}, \quad (14)$$

where L is the mechanical luminosity of the SNe cluster and $\zeta = Z/Z_\odot$ is the ISM metallicity in units of the solar value. Taking $L = N_e E_{\text{SN}}/t_e$,

$$R_c = 0.12 \text{ kpc} \left(\frac{N_e}{10} \right)^{\frac{4}{11}} \left(\frac{E_{\text{SN}}}{10^{51} \text{ erg}} \right)^{\frac{4}{11}} \left(\frac{t_e}{4 \times 10^7 \text{ yr}} \right)^{-\frac{4}{11}} \times \left(\frac{\lambda}{0.05} \right)^{\frac{28}{11}} \left(\frac{m_d}{0.17} \right)^{-\frac{14}{11}} \left(\frac{c_s}{10 \text{ km/s}} \right)^{-\frac{14}{11}} \times \left(\frac{M}{10^8 M_\odot} \right)^{-\frac{14}{33}} \left(\frac{1+z}{10} \right)^{-\frac{28}{11}} \left(\frac{\zeta}{0.05} \right)^{-\frac{27}{22}}. \quad (15)$$

Comparing equation (15) with equation (13) for R_e we find that the assumption of adiabatic expansion is valid in the

low mass galaxies thought to drive reionization. We therefore adopt equation (13) for R_e in the remainder of this paper.

In the limit where SNe evacuated regions are smaller than the scale height of the disk, and the starburst lifetime t_{SF} is much larger than the gas evacuation timescale t_e , the fraction F_{SN} of the SNe energy may be used in feedback suppressing subsequent star formation. However, if the SNe evacuated regions break out of the disk, or $t_{\text{SF}} < t_e$, not all of the energy will be available for feedback. Based on the ISM porosity model of Clarke & Oey (2002), a fraction $f_d = 2H/R_e$ of the SNe energy goes to increasing the ISM porosity for disks where $R_e > H$. In this case we find

$$f_d = 0.85 \left(\frac{N_e}{10} \right)^{-\frac{1}{3}} \left(\frac{E_{\text{SN}}}{10^{51} \text{ erg}} \right)^{-\frac{1}{3}} \left(\frac{\lambda}{0.05} \right)^{\frac{2}{3}} \left(\frac{m_d}{0.17} \right)^{-\frac{1}{3}} \times \left(\frac{M}{10^8 M_\odot} \right)^{-\frac{1}{9}} \left(\frac{1+z}{10} \right)^{-\frac{2}{3}} \left(\frac{c_s}{10 \text{ km/s}} \right)^2, \quad (16)$$

as long as $f_d < 1$ and $f_d = 1$ otherwise. Similarly, in cases where $t_{\text{SF}} < t_e \sim 4 \times 10^7$ yrs, only

$$f_t \equiv (t_{\text{SF}}/t_e)^2 \quad (17)$$

of the overall SNe energy output is generated by the time the starburst concludes. The quadratic dependence on time arises because the number of bubbles produced grows in proportion to time, while the maximum size of a bubble at time $t < t_e$ is also proportional to time (Oey & Clarke 1997). In cases where $t_{\text{SF}} > t_e$ we have $f_t = 1$.

In the next section we fit our model to the recent data of Smit et al. (2012) in order to constrain t_{SF} and f_* .

3 RESULTS

Observations of the star formation rate density function (SFRD) are plotted in Figure 1 for four different redshifts $z \sim 4, 5, 6$ and 7 . From these observations we constrain the two free parameters of our star formation model, $f_{*,\text{max}}$ and t_{SF} . We use the model to calculate SFRD functions for combinations of these parameters and calculate the χ^2 of the model as

$$\chi^2(f_{*,\text{max}}, t_{\text{SF}}) = \sum_{i=0}^{N_{\text{obs}}} \left(\frac{\log \Psi(\text{SFR}_i, f_{*,\text{max}}, t_{\text{SF}}, z) - \log \Psi_{\text{obs}}(\text{SFR}_i, z)}{\sigma_{\text{SFR}}(\text{SFR}_i, z)} \right)^2 \quad (18)$$

Here $\Psi_{\text{obs}}(\text{SFR}_i, f_{*,\text{max}}, t_{\text{SF}}, z)$ is the observed star formation rate density measured at redshift z , with uncertainty in dex of $\sigma_{\text{SFR}}(\text{SFR}_i)$. In calculating likelihoods at $z \sim 4$ and $z \sim 5$ we increased the quoted error bars by factors of 3 and 2 respectively in order to obtain a reduced χ^2 of order unity. The SFRD function is sensitive to the value of F_{SN} , and we therefore integrate the likelihood over a range of values uniformly distributed between $-1 < \log_{10} F_{\text{SN}} < 0$

$$\mathcal{L}(f_{*,\text{max}}, t_{\text{SF}}) \propto \int_{-1}^0 d(\log_{10} F_{\text{SN}}) e^{-\chi^2/2}. \quad (19)$$

We note that the relation between SFR and M in equation (1) is not perfect. As part of our comparison with observations, and to account for scatter in this relationship, we convolve the predicted SFRD function equation (2) with a Gaussian of width 0.5 dex in SFR . An intrinsic scatter of 0.5

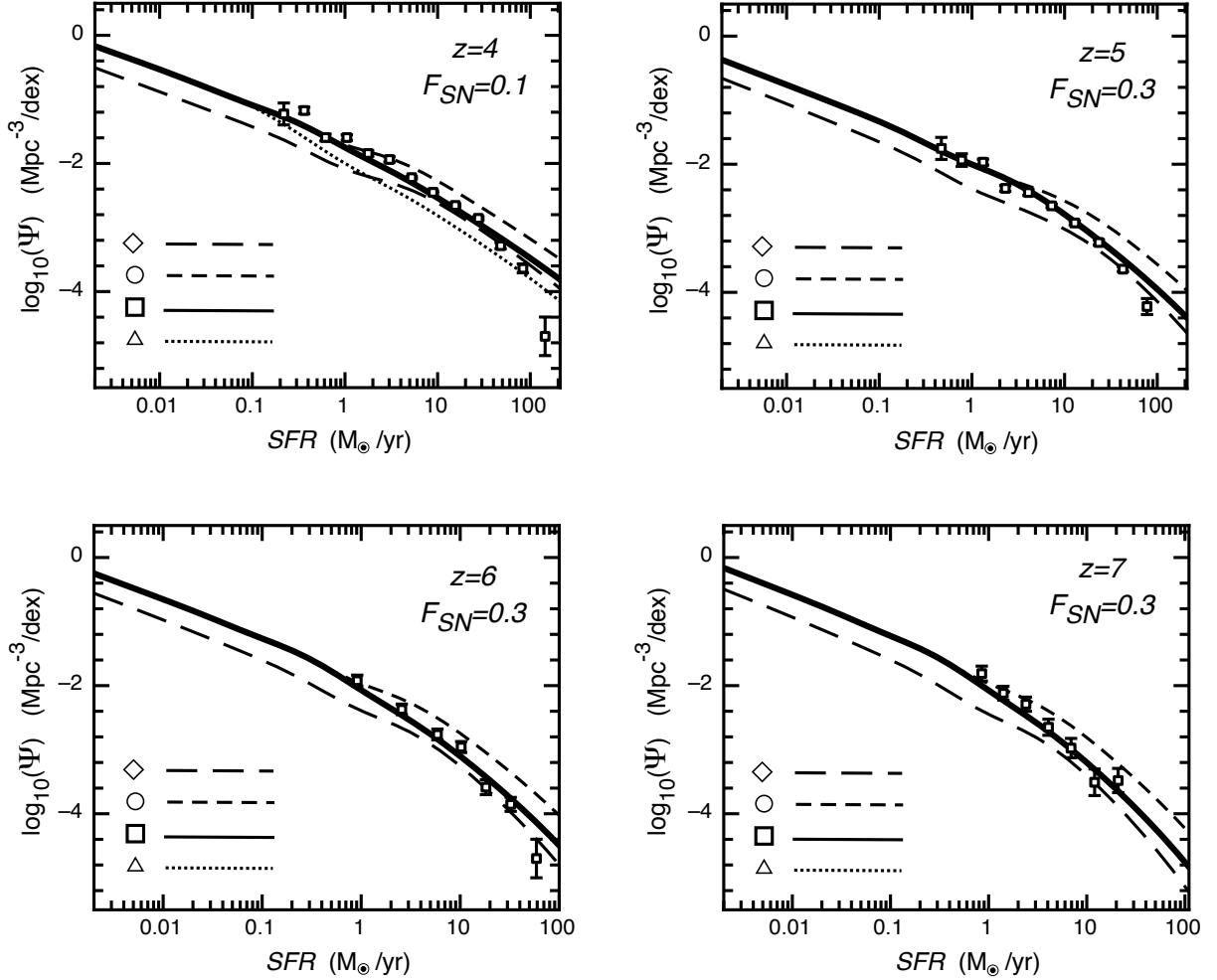


Figure 1. Comparison between the observed and modelled SFRD function (plotted as $\Psi = \ln 10 \times SFR \times \Phi$). The four panels show results for different redshift values. In each panel, the four curves correspond to a different choice of model parameters t_{SF} and $f_{*,max}$, labeled by the symbols in Figure 2. The thick solid lines represent values close to the best fit.

dex is motivated by the scatter in stellar mass at constant SFR found by González et al. (2011). However, in addition we find that the value of 0.5 dex provides the best statistical fit to the observations. Our qualitative results are not sensitive to the choice of this scatter, however.

3.1 Parameter constraints

Constraints on $f_{*,max}$ and t_{SF} for this model are shown in Figure 2. We note that these constraints are formal values assuming the particular model (for example, specifying the scale of a major merger). They are therefore indicative of the parameters describing the star formation model, whereas the overall uncertainty on starburst lifetime and efficiency may be larger than the ranges shown. We find that the shape of the SFRD function requires starburst durations of a few tens of Myr at $z \sim 5$, $z \sim 6$ and $z \sim 7$, with a few percent of the gas turned into stars per burst. For comparison the left and right hand vertical grey regions represent times smaller than the lifetime of the most massive stars

($t_s \sim 3 \times 10^6$ years), and times in excess of the lifetime of the least massive stars that produce SNe respectively. Our results therefore indicate that star formation in high redshift galaxies is terminated on the same timescale as feedback from SNe can be produced. The constraints can be understood qualitatively. First, larger values of $f_{*,max}$ at fixed t_{SF} lead to smaller values of halo mass at fixed SFR , and hence a larger SFRD function. Similarly, a longer starburst lifetime and hence duty cycle, implies that smaller halo masses are needed for a given value of SFR . Figure 1 shows the comparison between observed and modelled SFRD functions. The four curves shown correspond to model parameters t_{SF} and $f_{*,max}$ labeled by the symbols in Figure 2. We show the case of $F_{SN} = 0.3$, except at $z \sim 4$ where the lower value of $F_{SN} = 0.1$ produces a better fit. The thick solid lines provide the best fit to the observational data. The agreement with the data at multiple redshifts ($z = 5, 6$ and 7) is impressive since the values of $f_{*,max}$ and t_{SF} were kept fixed. We find that the SFRD function should continue to increase to much fainter levels than currently observed.

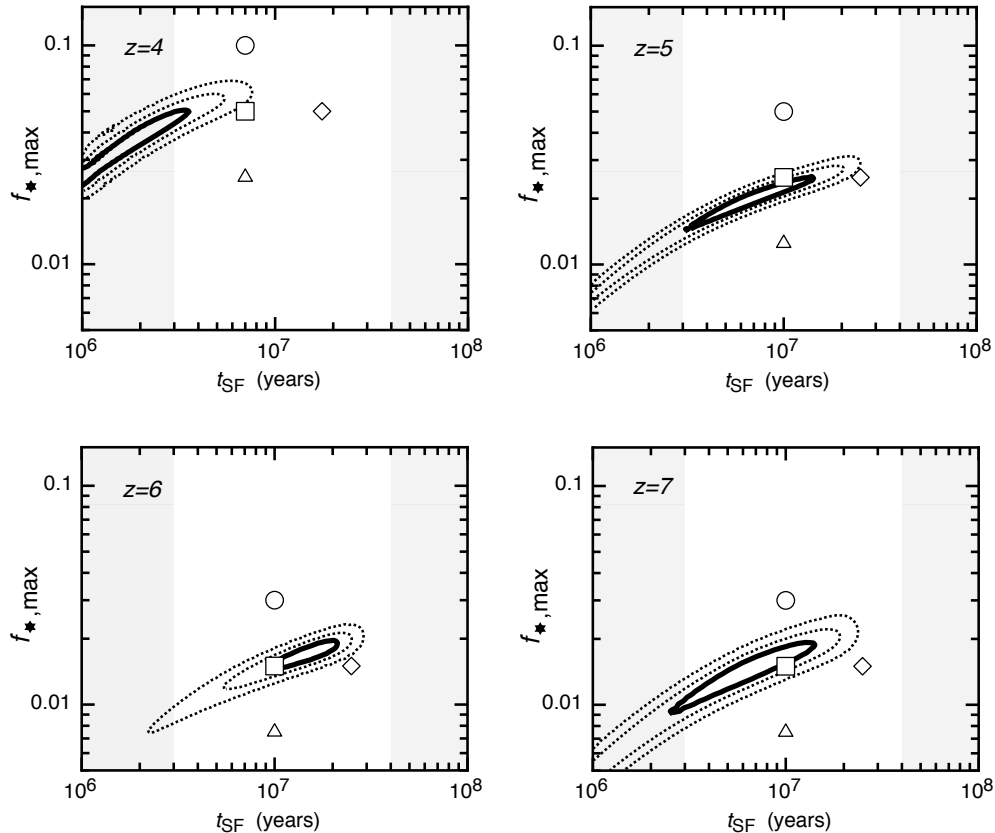


Figure 2. Constraints on the model parameters $f_{*,\max}$ and t_{SF} at four different redshifts (constraints are independent at each redshift). In each case, three contours are shown corresponding to differences in χ^2 relative to the best-fitting model of $\Delta\chi^2 = \chi^2 - \chi_{\text{min}}^2 = 1, 2.71$ and 6.63 . Projections of these contours on to the axes provide the 68.3, 90 and 99 per cent confidence intervals on individual parameter values. The vertical grey regions represent time-scales longer/shorter than the lifetime of the highest/lowest mass SNe progenitor ($3 \times 10^6 \text{yr} / 4 \times 10^7 \text{yr}$).

The parameters $f_{*,\max}$ and t_{SF} refer to single bursts, whereas our model includes multiple bursts at the rate of major mergers. We therefore calculate the total star formation efficiency $f_{*,\text{tot}} = N_{\text{merge}} f_*$ (i.e. the sum of f_* over all mergers), as well as the overall duty-cycle $N_{\text{merge}} t_{\text{SF}} / t_{\text{H}}$. These quantities are plotted in Figure 3 based on our model with parameter choices corresponding to the examples in Figure 1. We find duty-cycles of a few percent, with higher duty-cycles at higher redshift reflecting the increased ratio between the lifetime of massive stars and the age of the Universe. We find that ~ 5 – 10% of the gas forms stars in bright galaxies of $SFR \sim 1$ – $100 M_{\odot}$ per year, with lower fractions down to a percent in fainter galaxies.

3.2 The halo masses of star-forming galaxies

In Figure 4 we show the relation between SFR and halo mass M for galaxies based on our model with parameter choices corresponding to the examples in Figure 1. Galaxies observed to have $SFR \sim 1 M_{\odot}/\text{yr}$ reside in halos of $M \sim 10^{10} M_{\odot}$, a result consistent with previous work (e.g. Trenti

et al. 2010; Muñoz & Loeb 2011). Halos thought to host the smaller galaxies at the hydrogen cooling limit ($M \sim 10^{7.5} M_{\odot}$) are predicted to have low star formation rates of $SFR \sim 10^{-3} M_{\odot}/\text{yr}$.

3.3 The stellar masses of star-forming galaxies

In Figure 5 we show the relation between SFR and stellar mass $M_{\star} = m_{\text{d}} f_{*,\text{tot}} M$ for galaxies based on our model with parameter choices corresponding to the examples in Figure 1. $SFR \sim 1 M_{\odot}/\text{yr}$ characterise galaxies with $M_{\star} \sim 10^8 M_{\odot}$. Our model yields a close to linear relation between stellar mass and star formation rate, in good agreement with simulations (e.g. Jaacks et al. 2012; Salvaterra et al. 2011).

In Figure 5 we also show data points representing the mean relation between observed star formation rates and stellar masses. The relation between stellar masses and extinction-uncorrected star formation rates at $z \sim 4, 5$ and 6 , was presented in González et al. (2011). We have corrected these star formation rates for extinction using the methods outlined in Smit et al. (2012), based on relations in

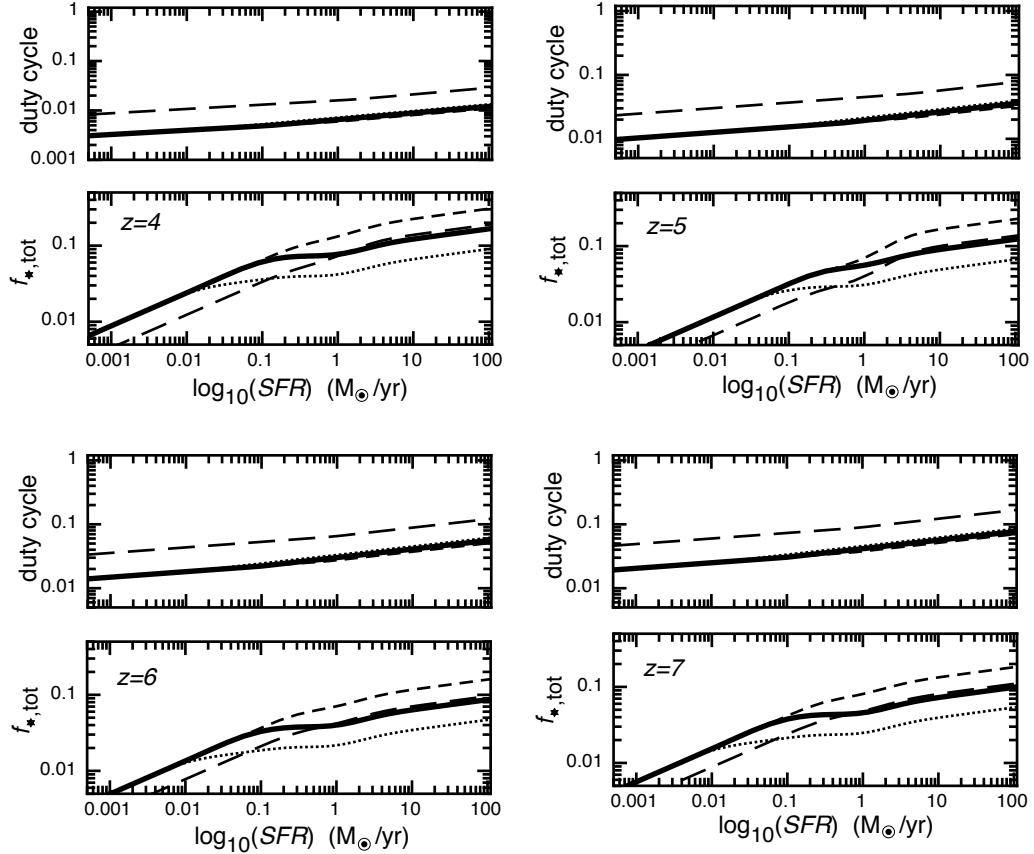


Figure 3. The values of total star formation efficiency $f_{*,\text{tot}}$ (i.e. the sum of f_* over all mergers), and the overall duty-cycle (i.e. the fraction of a Hubble time during which a galaxy is starbursting) as a function of SFR . The four curves shown correspond to the SFRD functions shown in Figure 1, with model parameters t_{SF} and $f_{*,\text{max}}$ designated by the symbols in Figure 2.

Meurer et al. (1999) and Bouwens et al. (2012). We find that our predicted $SFR - M_*$ relation is in agreement with the observations. In particular, we note that while the relation is fairly insensitive to the value of $f_{*,\text{max}}$, larger values of t_{SF} than suggested by our modelling of the SFRD function would imply a star formation rate at fixed stellar mass that is lower than required by the observations.

In Figure 6 we show the relations between the halo mass and stellar mass. The stellar to halo mass ratio is constant at high masses ($M \gtrsim 10^9 M_\odot$), but steeper towards low masses owing to the SNe feedback lowering the star formation efficiency in the model. Recently, Rocha et al. (2012) suggested that the Milky-Way dwarf spheroidals appear to have had their star formation quenched at the time of infall into the Milky-Way, and that this time of infall was typically $\sim 7 - 10$ Gyr ago. If true this implies that the Milky-Way dwarf spheroidals represent fossil records of the star-forming galaxies during reionization, and should have stellar masses described by our model. To make this comparison we therefore over-plot the observed relation for Milky-Way dwarf spheroidals (Boylan-Kolchin et al. 2012). To convert to halo mass we adopt the values of virial velocity at time of collapse from Boylan-Kolchin et al. (2012), and calculate the corresponding halo mass at each redshift z . We find

good agreement between the observed relation (although the scatter is large), indicating that if the dwarf spheroidals are old galaxies formed at around the end of reionization, then they would have the stellar to halo mass ratio predicted by our SNe feedback limited model. Combined with the correct prediction of the stellar mass for star-forming galaxies during reionization, this implies that our model correctly describes the stellar mass to halo mass ratio in the range $10^5 M_\odot \lesssim M_* \lesssim 10^{10} M_\odot$.

4 THE ESCAPE FRACTION OF IONIZING PHOTONS

The contribution of galaxies to reionization is dependent on the star formation rate and initial stellar mass function, but is also limited by the fraction of ionizing photons that escape their host galaxies. If the escape fraction is small, then star formation had to be very efficient at high redshift in order to reionize the Universe. The escape fraction is therefore a critical parameter in studies linking high redshift galaxy formation to reionization. In this section we discuss the implications of our model for the ionizing photon escape fraction.

Attempts to determine the ionizing photon escape frac-

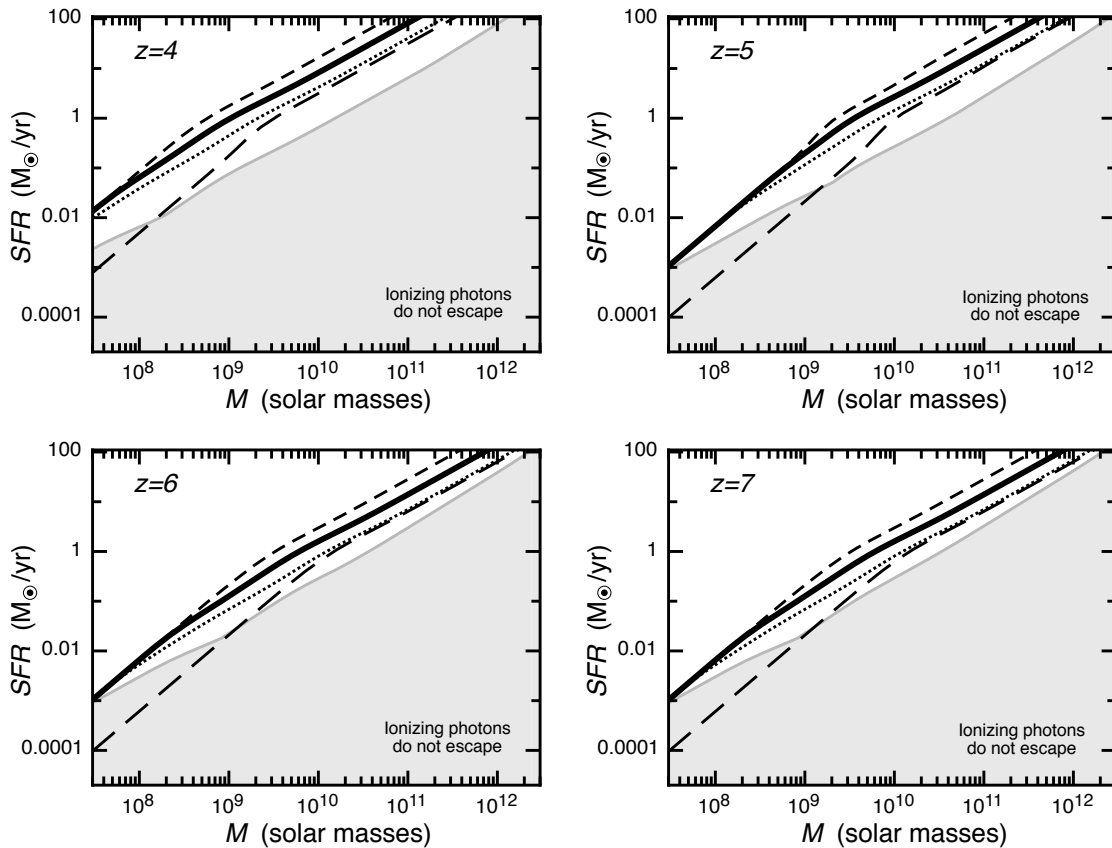


Figure 4. Relation between SFR and halo mass M at four different redshifts based on our model with parameter choices corresponding to the examples in Figure 1. Also shown is the critical star formation rate required to achieve porosity equal to unity (SFR_{crit}) as a function of halo mass. Regions of the $M - SFR$ plane where the porosity < 1 , and hence ionizing photons do not escape, are shaded grey.

tion have been dominated by direct observations of relatively low redshift galaxies, and by numerical simulation. Observational estimates of the escape fraction at the Lyman-limit are currently uncertain, with no confident detections at $0 < z < 1$, and only some detections at $z > 3$. At redshifts $z \sim 1 - 3$, observations have suggested a broad range of values for f_{esc} , from a few percent to $\gtrsim 20\%$ (Steidel et al. 2001; Fernández-Soto et al. 2003; Shapley et al. 2006; Siana et al. 2007, e.g.). Inoue et al. (2006) have examined the evolution of the escape fraction in the redshift range $z = 0 - 6$ using both direct observations of the escape fraction and values that they derive from measurements of the ionizing background. They find that the escape fraction evolves from $f_{esc} \sim 1 - 10\%$, increasing towards high redshift.

Theoretically, Razoumov & Sommer-Larsen (2006) used galaxy formation simulations incorporating high-resolution 3-D radiative transfer to show that the escape fraction evolves from $f_{esc} \sim 1-2\%$ at $z = 2.39$ to $f_{esc} \sim 6-10\%$ at $z = 3.6$. In agreement with Fujita et al. (2003), Razoumov & Sommer-Larsen (2006) (see also Yajima et al. 2009) find that increased supernova feedback at higher redshift expels gas from the vicinity of starbursting regions, creating tunnels in the galaxy through which ionizing photons can escape into the IGM. Numerical simulations (Gnedin et al. 2007) have predicted a value for f_{esc} between 1 and 3%, for halos of mass

$M \gtrsim 5 \times 10^{10} M_{\odot}$, over the redshift range $3 < z < 9$. This very low efficiency of reionization would have profound implications for the reionization history. In addition to a small escape fraction in massive galaxies, Gnedin et al. (2007) further predict that halos with $M \lesssim 5 \times 10^{10} M_{\odot}$ have an escape fraction that is negligibly small. However, more recently Wise & Cen (2009) have used a large suite of simulations to show that the time averaged escape fraction for dwarf galaxies is expected to be large ($> 25\%$). Since dwarf galaxies are thought to dominate the ionizing flux, resolution of this issue is of primary importance for studies of reionization. Overall, the escape fraction is predicted to span a very broad range, $0.01 \lesssim f_{esc} \lesssim 1$. This broad range may be explained by inhomogeneities in the hydrogen distribution within galaxies (Dove et al. 2000; Fernandez & Shull 2011), or by variations in viewing angle (Wood & Loeb 2000).

Within our formalism we follow Clarke & Oey (2002) who proposed that galaxies with a sufficient star formation rate to generate a porosity greater than unity had an escape fraction for ionizing photons that is of order unity, whereas galaxies with insufficient star formation have a negligible escape fraction. The critical star formation rate required to

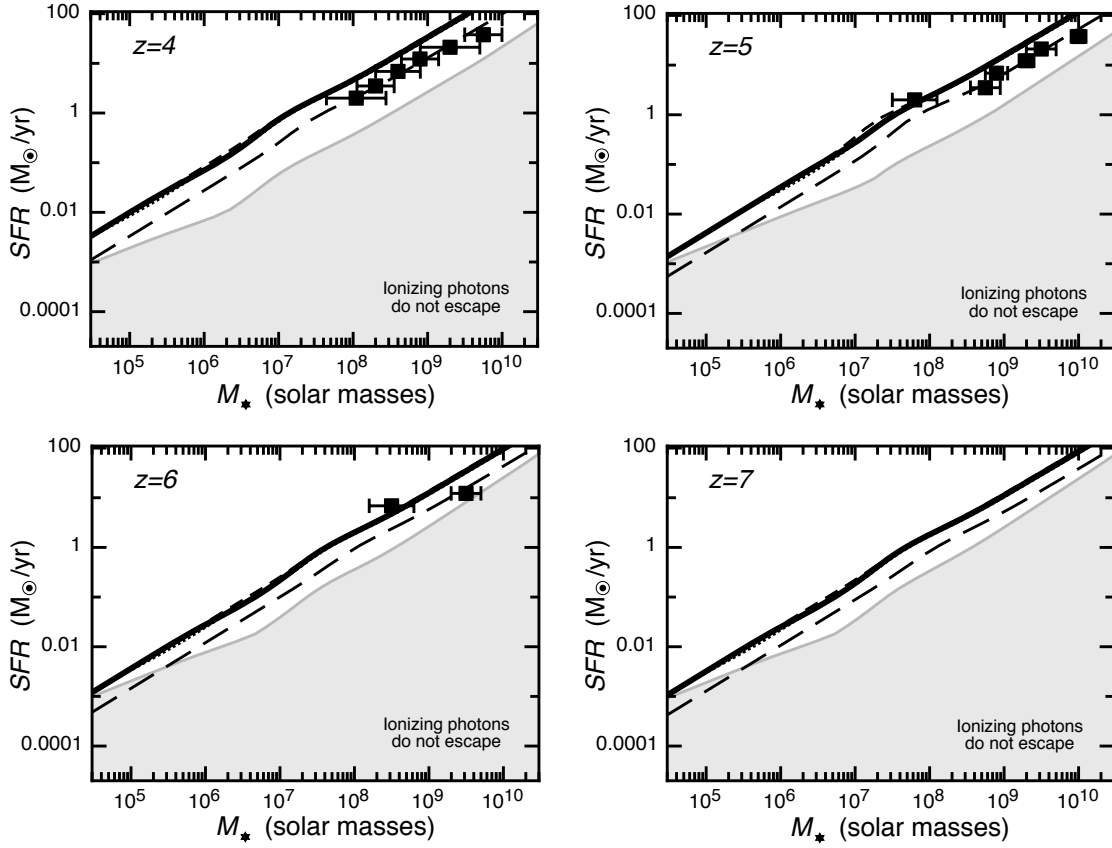


Figure 5. Relation between SFR and stellar mass M_* at four different redshifts based on our model with parameter choices corresponding to the examples in Figure 1. Also shown is the critical star formation rate required to achieve porosity of unity (SFR_{crit}) as a function of halo mass. Regions of the $M_* - SFR$ plane where the porosity < 1 , and hence ionizing photons do not escape are shaded grey. The points show the observed relations between stellar masses and star formation rates. We have corrected the star formation rates in González et al. (2011) for extinction using the methods outlined in Smit et al. (2012), based on relations in Meurer et al. (1999) and Bouwens et al. (2012).

achieve porosity of unity is (Clarke & Oey 2002)

$$SFR_{\text{crit}} = 0.15 M_{\odot} \text{yr}^{-1} (f_t f_d)^{-1} \left(\frac{m_d M}{10^{10} M_{\odot}} \right) \left(\frac{c_s}{10 \text{ km/s}} \right)^2. \quad (20)$$

In Figures 4 and 5 we plot the curves corresponding to SFR_{crit} as a function of halo mass and stellar mass, respectively. We shade the areas below the line for clarity to indicate the regions in the $M - SFR$ and $M_* - SFR$ planes where the porosity < 1 and hence ionizing photons do not escape. The model predicts that galaxies with halo masses in excess of $M \sim 10^8 M_{\odot}$ (corresponding to $M_* > 10^5 M_{\odot}$) have a sufficiently large SFR to potentially contribute to reionization.

In the model of Clarke & Oey (2002) galaxies with $SFR > SFR_{\text{crit}}$ attain porosity of unity after a time $t_Q = t_e (SFR/SFR_{\text{crit}})^{-1/2}$. The ionizing photon rate from a starburst drops rapidly once the most massive stars fade away on a timescale of $t_s \sim 3 \times 10^6$ years (Barkana & Loeb 2001). Since ionizing photons are produced for a time $t_{\text{SF}} + t_s$ but can only escape the galaxy after a time t_Q , the time during which the galaxy with $SFR > SFR_{\text{crit}}$ emits photons

into the IGM is

$$\begin{aligned} t_{\text{ion}} &= t_{\text{SF}} + t_s - t_Q \\ &= t_{\text{SF}} + t_s \left(1 - \left(\frac{t_e}{t_s} \right) \left(\frac{SFR}{SFR_{\text{crit}}} \right)^{-1/2} \right). \end{aligned} \quad (21)$$

For small values of $t_{\text{SB}} < t_e$, Q may never reach unity for some values of SFR , even if $SFR > SFR_{\text{crit}}$. To estimate t_{ion} we must therefore integrate over the distribution for SFR at fixed halo mass, which was assumed to have a scatter of 0.5dex. Thus we calculate

$$\langle t_{\text{ion}} \rangle = \int d\Delta_{SFR} t_{\text{ion}}(SFR \times 10^{\Delta_{SFR}}) e^{-\frac{(\Delta_{SFR})^2}{2 \times 0.5^2}}. \quad (22)$$

We note that since $\langle t_{\text{ion}} \rangle < t_{\text{SF}} + t_s$, we expect a wide range of observed escape fractions for star forming galaxies depending on whether or not the starburst is being observed before or after t_Q . The galactic porosity model of (Clarke & Oey 2002) postulated that the escape fraction is negligible at $t < t_Q$ and of order unity at $t > t_Q$. Our model provides the probability P_{ion} that a galaxy with a particular SFR should be observed with a non-zero escape fraction for ionizing radiation, calculated as the fraction of time that the

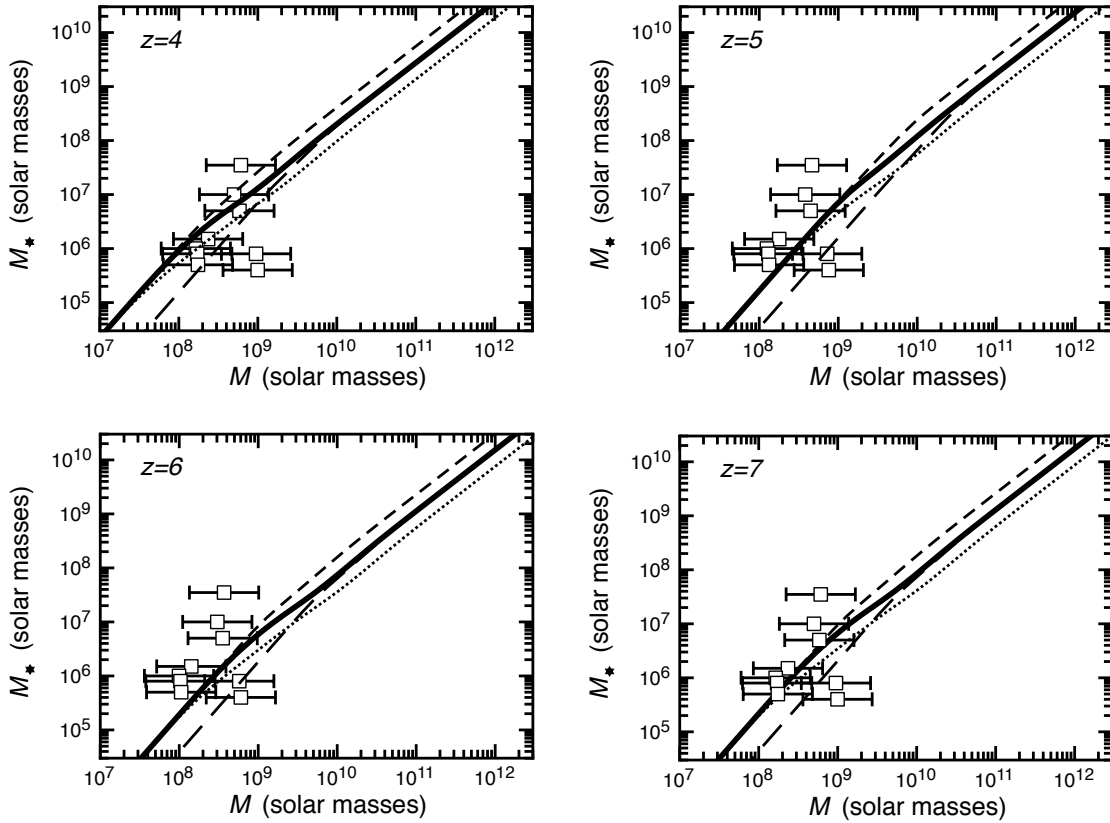


Figure 6. Relation between halo mass M and stellar mass M_* at four different redshifts based on our model with parameter choices corresponding to the examples in Figure 1. The data points are based on the relation between stellar mass and maximum circular velocity for Milky-Way dwarf spheroidals (Boylan-Kolchin et al. 2012). To convert to halo mass we adopt the values of virial velocity at time of collapse from Boylan-Kolchin et al. (2012), and calculate the corresponding halo mass at redshift z .

galaxy is observed to be star-forming and for which $t > t_Q$,

$$P_{\text{ion}} = \frac{\langle t_{\text{ion}} \rangle}{t_{\text{SF}} + t_s}. \quad (23)$$

Curves of P_{ion} are plotted as a function of SFR in Figure 7. The left hand panel shows the best fit case of $t_{\text{SF}} = 10^7$ yr, and the right hand panel $t_{\text{SF}} = 2 \times 10^7$ yr. Four redshifts are shown. Our model predicts that large escape fractions should be rare for both low SFR and high SFR galaxies. However, we expect approximately a half of star-forming galaxies with $SFR \sim 0.1 - 1 M_{\odot}/\text{yr}$ to have a significant escape fraction. Thus, our model provides a natural explanation for the wide range of conclusions regarding observations of the escape fraction of ionizing photons from star-forming galaxies.

Next we investigate the implications of this model for the reionization history.

5 IMPLICATIONS FOR THE REIONIZATION HISTORY

We continue with a semi-analytic calculation of the reionization history of the IGM based on the star formation model presented in § 2. The basis for our model of reionization is the excess ionization rate over the recombination rate for hydrogen in an inhomogeneous IGM. Miralda-Escudé et al.

(2000) presented a model that allows the calculation of an effective recombination rate in an inhomogeneous universe by assuming a maximum overdensity (Δ_c) penetrated by ionizing photons within HII regions. The model assumes that reionization progresses rapidly through islands of lower density prior to the overlap of individual cosmological ionized regions. Following the overlap epoch, the remaining regions of high density are gradually ionized. It is therefore hypothesized that at any time, regions with gas below some critical overdensity $\Delta_i \equiv \rho_i / \langle \rho \rangle$ are highly ionized while regions of higher density are not. The fraction of mass in regions with overdensity below Δ_i , is found from the integral

$$F_M(\Delta_i) = \int_0^{\Delta_i} d\Delta P_V(\Delta) \Delta, \quad (24)$$

where $P_V(\Delta)$ is the volume weighted probability distribution for Δ . Miralda-Escudé et al. (2000) quote a fitting function that provides a good fit to the volume weighted probability distribution for the baryon density in cosmological hydrodynamical simulations. In what follows, we draw primarily from the prescription of Miralda-Escudé et al. (2000) and refer the reader to the original paper for a detailed discussion of its motivations and assumptions. Wyithe & Loeb (2003a) employed this prescription within a semi-analytic model of reionization. This model was extended by Srbinsky &

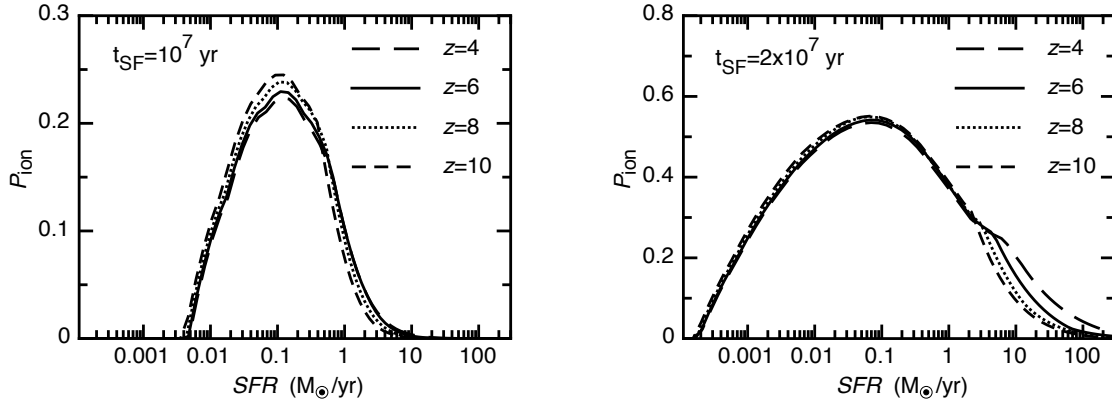


Figure 7. Curves of P_{ion} as a function of SFR . The left hand panel shows the of $t_{\text{SF}} = 10^7$ yr corresponding to the best fit example in Figure 1. The right hand panel shows the larger value of $t_{\text{SF}} = 2 \times 10^7$ yr. In each case curves are shown for $z \sim 4, 6, 8$ and 10 .

Wyithe (2007) and by Wyithe et al. (2008). We refer the reader to those papers for a full description.

The quantity Q_i is defined to be the volume filling factor within which all matter at densities below Δ_i has been ionized. The reionization history is quantified by the evolution of Q_i that follows the rate equation

$$\frac{dQ_i}{dz} = \frac{1}{n_0 F_M(\Delta_i)} \frac{dn_\gamma}{dz} - \left[\alpha_B (1+z)^3 R(\Delta_i) n_0 \frac{dt}{dz} + \frac{dF_M(\Delta_i)}{dz} \right] \frac{Q_i}{F_M(\Delta_i)} \quad (25)$$

where α_B is the case B recombination coefficient, n_0 is the mean comoving density of hydrogen in the IGM, and $R(\Delta_i)$ is the effective clumping factor of the IGM. The evolution is driven by the rate of emission of ionizing photons per comoving volume dn_γ/dz . Within this formalism, the epoch of overlap is precisely defined as the time when Q_i reaches unity. Prior to the overlap epoch we must solve for both Q_i and F_M (or equivalently Δ_i). The relative growth of these depends on the luminosity function and spatial distribution of the sources. In this regime we assume Δ_i to be constant with redshift before the overlap epoch and compute results for models with values of $\Delta_i \equiv \Delta_c = 10$. Different values of Δ_c are not found to quantitatively effect our results for values in the range $5 < \Delta_c < 20$ (Wyithe et al. 2008).

Following overlap we may describe the post-overlap evolution of the IGM by computing the evolution of the ionized mass fraction according to the equation

$$\frac{dF_M(\Delta_i)}{dz} = \frac{1}{n_0} \frac{dn_\gamma}{dz} - \alpha_B (1+z)^3 R(\Delta_i) n_0 \frac{dt}{dz}. \quad (26)$$

This follows directly from equation (25) with $Q_i = 1$. In this post overlap regime the value of Δ_i is the dependent variable describing the ionization state of the IGM (whereas prior to overlap $\Delta_i = \Delta_c$). Equation (26) is integrated to obtain F_M (or equivalently Δ_i) as a function of redshift.

The emission rate of ionizing photons per co-moving volume that is required to compute the reionization history can be written

$$\frac{dn_\gamma}{dz} = N_\gamma \frac{\langle f_{\text{esc}} \dot{\rho}_* \rangle}{m_p} \frac{dt}{dz}, \quad (27)$$

where N_γ is the number of ionizing photons produced per

baryon incorporated into stars, and $\langle f_{\text{esc}} \dot{\rho}_* \rangle$ is the product of the escape fraction and the star formation rate density averaged over halo mass. As described in the introduction, only a fraction f_{esc} of the ionizing photons produced by stars enter the IGM. We define $\langle \dot{\rho}_{*,\text{esc}} \rangle$ using our formalism as

$$\langle f_{\text{esc}} \dot{\rho}_* \rangle_{>M_1} = \int_{M_1}^{\infty} dM f_{\text{esc}} SFR \times \frac{\langle t_{\text{ion}} \rangle}{t_H} \left(t_H \Delta M \frac{dN_{\text{merge}}^2}{dt d\Delta M} \Big|_{M_1, \Delta M} \frac{dn}{dM} \right),$$

where $\langle t_{\text{ion}} \rangle$ is the time during which the galaxy emits ionizing photons into the IGM (equation 22).

In a cold neutral IGM beyond the redshift of reionization, the collapsed fraction should be computed for halos of sufficient mass to initiate star formation. The minimum virial temperature is set by the temperature $T_{\text{min}} \sim 10^4$ K, above which atomic hydrogen cooling promotes star formation. Following the reionization of a region, the Jeans mass in the heated IGM limits accretion to halos above $T_{\text{ion}} \sim 10^5$ K (Efsthathiou 1992; Thoul & Weinberg 1996; Dijkstra et al. 2004). Including these separate components from ionized and neutral regions of IGM, we get

$$\langle f_{\text{esc}} \dot{\rho}_* \rangle = \langle f_{\text{esc}} \dot{\rho}_* \rangle_{>M_{\text{min}}} (1 - Q_i) + \langle f_{\text{esc}} \dot{\rho}_* \rangle_{>M_{\text{ion}}} Q_i, \quad (28)$$

Our model assumes a spectral energy distribution of Population-II stars with a metallicity $Z = 0.05 Z_\odot$ and a Scalo (1998) initial mass function, for which the resulting number of hydrogen ionizing photons per baryon incorporated into stars is $N_\gamma \sim 4000$ (Barkana & Loeb 2001).

In order to estimate the ionizing background following the end of reionization, we compute a reionization history given a particular value of Δ_c , combined with assumed values for f_* and f_{esc} . Given this history, we then compute the evolution of the background radiation field due to the same sources. After the overlap epoch, ionizing photons will experience attenuation due to residual over dense pockets of HI gas. We use the prescription of Miralda-Escudé et al. (2000) to estimate the ionizing photon mean-free-path. Following Oh & Furlanetto (2005), who note that the the constant of proportionality relating mean-free-path to the volume-filling fraction should be reduced by approximately a factor of 2, we adopt $\lambda = (30 \text{ km s}^{-1})/H(1-Q)^{-2/3}$, and subsequently derive the attenuation of ionizing photons. We then compute

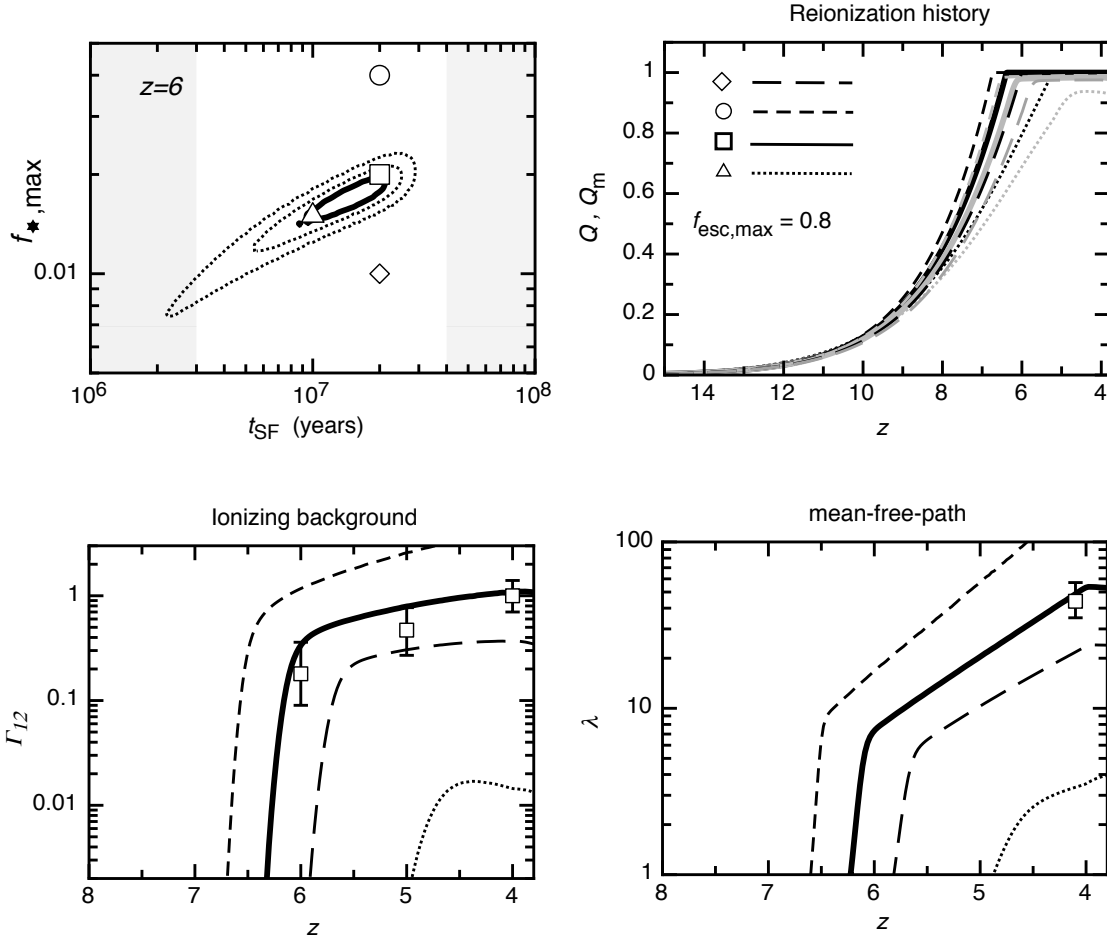


Figure 8. Models for the reionization of the IGM and the subsequent post-overlap evolution of the ionizing radiation field. Four cases are shown, with line styles corresponding to the cases over plotted on the constraints on $f_{*,\max}$ and t_{SF} at $z \sim 6$ that are repeated in the top left panel for reference. A value of $\Delta_c = 10$ was adopted for the critical overdensity prior to the overlap epoch. *Upper Right Panel:* the evolution of volume averaged (dark lines) and mass averaged (grey lines) neutral hydrogen fraction. *Lower Left Panel:* Ionization rate as a function of redshift (in units of 10^{-12}s^{-1}). The observational points are from Bolton & Haehnelt (2007) and Wyithe & Bolton (2011). *Lower Right Panel:* The mean-free-path for ionizing photons. The data point is based on Storrie-Lombardi et al. (1994).

the flux at the Lyman-limit in the IGM due to sources immediate to each epoch, in addition to redshifted contributions from earlier epochs.

We show the results of this modelling in Figure 8 for four models, including the best-fit case presented in Figure 1. For reference the constraints on $f_{*,\max}$ and t_{SF} at $z \sim 6$ are repeated in the top left panel. The upper right panel shows the evolution of volume averaged (dark lines) and mass averaged (grey lines) neutral hydrogen fraction. To illustrate that the model for star formation is consistent with the reionization history, we also show the observables of ionization rate as a function of redshift (lower left), and the mean-free-path for ionizing photons (lower right). We find for a choice of $f_{\text{esc}} = 0.8$, that a model near the best fit for the SFRD function ($t_{\text{SF}} = 2 \times 10^7\text{yr}$) results in a reionization history that is consistent with low redshift constraints (thick lines). The reionization history shown is consistent with recent constraints from the patchy kinetic Sunyaev-Zel'dovich effect (Zahn et al. 2012). The model produces an optical depth to electron scattering of $\tau_{\text{es}} = 0.065$, which is lower than the observed value of $\tau_{\text{es}} = 0.088 \pm 0.015$ (Ko-

matsu et al. 2011). However, our model does not include the possibilities of population-III stars or an increased escape fractions at very high redshift (Alvarez et al. 2012). Models with larger $f_{*,\max}$ reionize the universe too early, while those with smaller $f_{*,\max}$ or larger t_{SF} reionize the universe too late. For the model with a smaller value of $t_{\text{SF}} = 10^7\text{yr}$, we find that reionization occurs very late (at $z \sim 5$), and greatly underestimates the ionizing background. This is because porosity of unity is rarely achieved by the time the starburst is finished in this model, so that very few ionizing photons escape. This indicates that the reionization of the IGM may limit the starburst time-scale to be $t_{\text{SF}} \gtrsim 10^7\text{yr}$.

In the left panel of Figure 9 we show the *SFR* weighted average of the escape fraction (i.e. $\langle f_{\text{esc}} \rangle_{\text{SFR}} \equiv \langle f_{\text{esc}} \dot{\rho}_* \rangle / \langle \dot{\rho}_* \rangle$) as a function of redshift for the four models shown in Figure 8. Since the value of escape fraction in highly star forming galaxies is $f_{\text{esc}} = 0.8$ in this model, we find that most ionizing photons produced in galaxies are being lost either because the *SFR* was insufficient to attain porosity equal to unity, or because the UV luminous stars had died before porosity of unity was achieved. Interestingly,

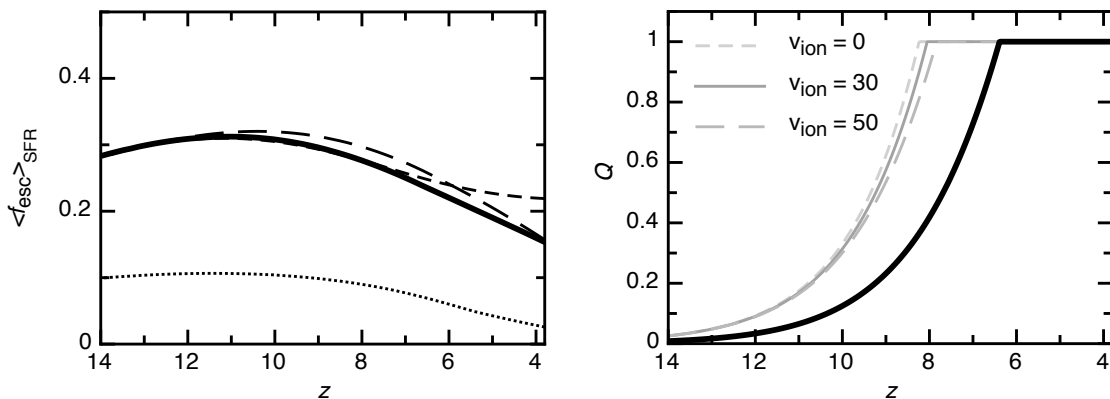


Figure 9. Contribution of galaxies to reionization. *Left Panel:* The evolution of *SFR* weighted average escape fraction for the four models shown in Figure 8. *Right Panel:* The evolution of volume averaged neutral fraction. Three cases are shown, including the best fit model from Figure 8 (thick black line) for comparison with models in which photons are allowed to escape from all galaxies, with $f_{\text{esc}} = 0.8$ (i.e. $SFR_{\text{crit}} = 0$). In these cases we show examples where radiative feedback is included ($v_{\text{ion}} = 30\text{km/s}$ and $v_{\text{ion}} = 50\text{km/s}$), and a case in which it is not (i.e. $v_{\text{ion}} = 0$).

we find that the SFR averaged escape fraction increases towards high redshift, being twice as large at $z \sim 10$ as at $z \sim 4$. This trend is consistent both with the requirements of the Ly α forest at $z \sim 4$ (Bolton & Haehnelt 2007), and recent empirical estimates for the escape fraction of ionizing photons from high redshift galaxies during reionization (Finkelstein et al. 2012).

6 THE CONTRIBUTION OF LOW MASS GALAXIES TO REIONIZATION

A range of models (e.g. Haiman & Holder 2003; Iliev et al. 2007) have predicted that radiative feedback, which can suppress star formation in very low mass galaxies, will have a significant effect on the reionization history. The effect is often referred to as self regulation of reionization, because it could lead to the reionization process being extended. In these models reionization is predicted to start at high redshift due to very low mass galaxies with virial temperatures of $\sim 10^4\text{K}$. However, once regions become ionized subsequent star formation in these very low mass galaxies is quenched, so that reionization must be completed by galaxies with a virial temperature $\gtrsim 10^5\text{K}$ which form later. The reason why radiative feedback could have a large effect on the reionization history is well understood. At high redshift the collapsed fraction of dark matter halos is dominated by low mass galaxies with a virial temperatures smaller than $\sim 10^5\text{K}$. Despite the focus of numerical and semi-analytic studies of high redshift galaxy formation on the role of feedback on star formation in low mass galaxies (e.g. Raičević et al. 2011; Finlator et al. 2011), models of the structure of reionization have generally assumed the luminosity to be proportional to halo mass, and that the escape fraction of ionizing photons is independent of mass (e.g. Iliev et al. 2007; McQuinn et al. 2007). As a result, the ionizing photon budget for reionization in these constant mass-to-light models is also dominated by low mass galaxies prior to reionization. However, in this paper we have found that SNe feedback is required to reproduce the shape of the high redshift

SFRD function, in agreement with the previous numerical work. Thus, the contribution to reionization from low mass galaxies may be smaller than previously thought (Raičević et al. 2011). In this section, we investigate the contribution to reionization from galaxies of various masses.

The effect of low mass galaxies on the reionization history is illustrated in the right panel of Figure 9 which shows the evolution of volume averaged neutral fraction. The best fit model from Figure 8 is shown (thick black line) for comparison with models in which the critical SFR criteria for ionizing photons to escape is not applied so that photons are allowed to escape from all galaxies with $f_{\text{esc}} = 0.8$ (grey lines). For the latter, three cases are shown including where radiative feedback is not included (i.e. $v_{\text{ion}} = 0$) and where $v_{\text{ion}} = 30\text{km/s}$ and $v_{\text{ion}} = 50\text{km/s}$. We see that the application of the critical SFR criteria has a significant effect on the reionization history, leading to an earlier reionization by $\Delta z \sim 1.5$ at a fixed f_{esc} . However, suppression of galaxies smaller than $v_{\text{ion}} = 30\text{km/s}$ or 50km/s results in a smaller change to the reionization history relative to a model in which radiative feedback does not operate ($\Delta z \lesssim 0.2$), a finding that is contrary to the standard picture for self-regulated reionization (e.g. Iliev et al. 2007).

To understand the reasons for this we show the cumulative contribution to the number of ionizing photons per hydrogen in the Universe per Hubble time as a function of halo virial velocity (left panel of Figure 10). In calculating these curves we have not applied the SFR_{crit} criteria (equation 20), and assumed that ionizing photons escape all galaxies with f_{esc} . Contributions at three different redshifts are shown. In the right panel we repeat these results, but plot the contributions as a function of star formation rate rather than virial velocity. We find that photons from galaxies below $v_{\text{vir}} \sim 30\text{km/s}$ (with $SFR \lesssim 0.01M_{\odot}/\text{yr}$), corresponding to those affected by radiative feedback, represent only $\sim 10\%$ of the potential photon budget at $z \sim 6$ and only $\sim 30\%$ at $z \sim 10$. Thus, these low mass galaxies make only a small contribution to reionization, implying that radiative feedback should not be important in regulating the

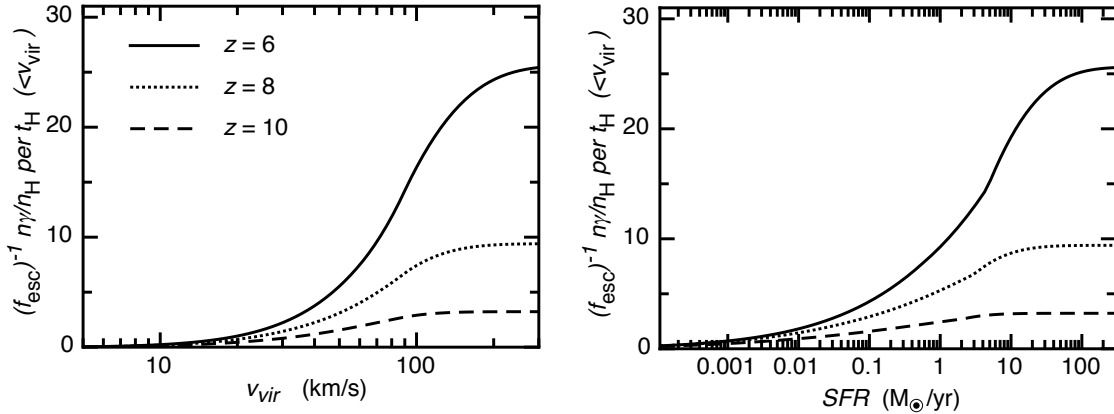


Figure 10. Contribution of low mass galaxies to reionization. *Left Panel:* The cumulative contribution to the number of ionizing photons per hydrogen in the Universe as a function of halo virial velocity. To investigate the possible contribution to reionization from small galaxies we have not applied the SFR_{crit} criteria, and instead assumed that ionizing photons escape all galaxies with $f_{\text{esc}} = 0.8$. Contributions at three different redshifts are shown, and expressed in units of photons per hydrogen in the IGM times f_{esc}^{-1} (in order to make the curves independent of f_{esc}). *Right Panel:* Results repeated as a function of the SFR per galaxy.

reionization process. This reduced contribution arises because SNe have lowered the star formation efficiency to a level where galaxies with $v_{\text{vir}} \sim 10 \text{ km/s}$ contribute a very small fraction of the total star formation rate, despite the corresponding halos representing the dominant component of collapsed fraction of dark matter.

Thus, we conclude that SNe feedback was much more important than radiative feedback in shaping the reionization history, a result that is consistent with both Raićević et al. (2011) and the recent semi-analytic modelling of Kim et al. (2012) using GALFORM within the Millennium-II simulation. We note that an important caveat to these results is the possibility of a top-heavy mass function of Population-III stars in small galaxies. Since in this case the ionizing efficiency is much larger than for Population-II stars, Population-III stars in early low-mass galaxies could make a more important contribution to reionization, partially reionizing the Universe at earlier times (e.g. Wyithe & Loeb 2003a; Cen 2003). Overall we find that half of the ionizing photons are produced by galaxies with $v_{\text{vir}} \gtrsim 60 \text{ km/s}$ corresponding to $SFR \gtrsim 1 M_{\odot}/\text{yr}$. These are observed galaxies, indicating that observations summarised in Smit et al. (2012) correspond to about half of the ionizing photons produced by galaxies. This result is consistent with the recent findings of Finkelstein et al. (2012), who suggested that the observed population of $z \sim 6$ galaxies is sufficient to provide most of the ionizing photons required for reionization assuming escape fractions below 50%.

7 CONCLUSION

We have described a simple model for the star formation rate density function at high redshifts based on the extended Press-Schechter formalism. This model assumes that a starburst is triggered by each major merger, lasting for a time t_{SF} and converting at most $f_{\star, \text{max}}$ of galactic gas into stars. We include a simple physical prescription for SNe feedback based on the galactic porosity model of Clarke & Oey (2002)

that suppresses star formation in low mass galaxies, and results in a minimum galaxy mass from which ionizing photons can escape. This model for star formation has only two free parameters, t_{SF} and $f_{\star, \text{max}}$, but accurately describes recent measurements of the amplitude and shape of the star formation rate density function between redshifts 4 and 7.

Comparison of our modelling with observational data implies that individual starbursts were terminated after $t_{\text{SF}} \sim 2 \times 10^7$ years. This termination time lies between the main-sequence lifetimes of the lowest and highest mass SNe progenitors, indicating that starbursts were quenched once SNe feedback had time to develop. From the sum of all major merger events, high redshift galaxies convert $\sim 5 - 10\%$ of their mass into stars for large galaxies with star formation rates above $\sim 1 M_{\odot}/\text{yr}$. However, the overall star formation efficiency of lower luminosity galaxies is only a few percent. In our model, high redshift galaxies have a high duty-cycle for star formation, undergoing starbursts $\sim 10\%$ of the time at $z \sim 10$.

We calculate the relation between stellar mass and star formation rate, finding it to be approximately linear, in agreement with previous theoretical work and observations. The predicted ratio of star formation rate to stellar mass based on our fit to the star formation rate density function agrees with the observed values for star-forming galaxies at $z \sim 4-6$ where stellar mass has been measured. Moreover, if the Milky-Way dwarf spheroidals represent fossil records of the star-forming galaxies during reionization (Rocha et al. 2012), they should also have stellar masses described by our model and we find good agreement with the predicted relation between stellar and halo masses (although the scatter is large). This implies that our model correctly describes the stellar mass to halo mass ratio from $10^5 M_{\odot} \lesssim M_{\star} \lesssim 10^{10} M_{\odot}$.

We used our model to discuss the escape fraction of ionizing photons from high redshift star-forming galaxies. Clarke & Oey (2002) proposed a simple model where galaxies with a sufficient star formation rate to generate a porosity greater than unity had an escape fraction for ionizing photons that is of order unity, whereas galaxies with insuffi-

cient star formation have a negligible escape fraction. Since a fraction of the galaxies starburst lifetime is required to build the porosity to unity, every star-forming galaxy has a non-zero probability of being observed with a zero escape fraction for ionizing radiation. Our model predicts that large escape fractions should be rare for both low SFR and high SFR galaxies. However, we expect approximately a half of star-forming galaxies with $SFR \sim 0.1 - 1M_{\odot}/\text{yr}$ to have significant escape fraction. Thus our model provides a natural explanation for the wide range of conclusions regarding observations of the escape fraction of ionizing photons from star-forming galaxies (Steidel et al. 2001; Fernández-Soto et al. 2003; Shapley et al. 2006; Siana et al. 2007, e.g.), and predicts that the escape fraction during reionization at $z \sim 10$ was twice as large as at $z \sim 4$.

We also used a semi-analytic model for the reionization process based on our SNe regulated star formation history. Even after allowing for the fact that SNe feedback enables escape of ionizing radiation only after the galactic porosity reaches unity, we find that our model is able to reionize the Universe within current observational constraints. We find that low mass galaxies were minor contributors to reionization, owing to the suppression of star formation by SNe feedback. We further find that this SNe feedback lowers the efficiency of star formation in low mass galaxies to such an extent that photo-ionization feedback on low mass galaxy formation does not significantly effect the reionization history. This is because the galaxies that would have been subject to radiative feedback are only very minor contributors to the potential ionizing photon budget once SNe feedback is taken into account.² Finally, we find that approximately half of the ionizing photons needed to complete reionization have already been observed in star-forming galaxies at $z = 6-10$.

Acknowledgments We thank Jamie Bolton for helpful discussions. JSBW acknowledges the support of the Australian Research Council. AL was supported in part by NSF grant AST-0907890 and NASA grants NNX08AL43G and NNA09DB30A.

REFERENCES

- Alvarez M. A., Finlator K., Trenti M., 2012, *astro-ph/1209.1387*
- Barkana R., Loeb A., 2001, *ApJS*, 349, 125
- Bell E. F., de Jong R. S., 2001, *ApJ*, 550, 212
- Benson A. J., Sugiyama N., Nusser A., Lacey C. G., 2006, *MNRAS*, 369, 1055
- Bolton J. S., Haehnelt M. G., 2007, *MNRAS*, p. 957
- Bouwens R. J., Illingworth G. D., Oesch P. A., Franx M., Labbé I., Trenti M., van Dokkum P., Carollo C. M., González V., Smit R., Magee D., 2012, *ApJ*, 754, 83
- Bouwens R. J., Illingworth G. D., Oesch P. A., Labbé I., Trenti M., van Dokkum P., Franx M., Stiavelli M., Carollo C. M., Magee D., Gonzalez V., 2011, *ApJ*, 737, 90
- Boylan-Kolchin M., Bullock J. S., Kaplinghat M., 2012, *MNRAS*, 422, 1203
- Cen R., 2003, *ApJL*, 591, L5
- Clarke C., Oey M. S., 2002, *MNRAS*, 337, 1299
- Dekel A., Woo J., 2003, *MNRAS*, 344, 1131
- Dijkstra M., Haiman Z., Rees M. J., Weinberg D. H., 2004, *ApJ*, 601, 666
- Dove J. B., Shull J. M., Ferrara A., 2000, *ApJ*, 531, 846
- Efstathiou G., 1992, *MNRAS*, 256, 43
- Fakhouri O., Ma C.-P., Boylan-Kolchin M., 2010, *MNRAS*, 406, 2267
- Fernandez E. R., Shull J. M., 2011, *ApJ*, 731, 20
- Fernández-Soto A., Lanzetta K. M., Chen H.-W., 2003, *MNRAS*, 342, 1215
- Finkelstein S. L., Papovich C., Ryan Jr. R. E., Pawlik A. H., Dickinson M., Ferguson H. C., Finlator K., Koekoemoer A. M., Gialavalisco M., Cooray A., Dunlop J. S., Faber S. M., Grogin N. A., Kocevski D. D., Newman J. A., 2012, *ArXiv e-prints*
- Finlator K., Oppenheimer B. D., Davé R., 2011, *MNRAS*, 410, 1703
- Fujita A., Martin C. L., Mac Low M.-M., Abel T., 2003, *ApJ*, 599, 50
- Gnedin N. Y., Kravtsov A. V., Chen H.-W., 2007, *ArXiv e-prints*, *astro-ph/0707.0879*
- González V., Labbé I., Bouwens R. J., Illingworth G., Franx M., Kriek M., 2011, *ApJL*, 735, L34
- Haiman Z., Holder G. P., 2003, *ApJ*, 595, 1
- Iliev I. T., Mellema G., Shapiro P. R., Pen U.-L., 2007, *MNRAS*, 376, 534
- Inoue A. K., Iwata I., Deharveng J.-M., 2006, *MNRAS*, 371, L1
- Jaacks J., Nagamine K., Choi J.-H., 2012, *ArXiv e-prints*
- Kauffmann G., Heckman T. M., White S. D. M., Charlot S., Tremonti C., Peng E. W., Seibert M., Brinkmann J., Nichol R. C., SubbaRao M., York D., 2003, *MNRAS*, 341, 54
- Kim H.-S., Wyithe J. S. B., Raskutti S., Lacey C. G., 2012, *ArXiv e-prints*
- Komatsu E., Smith K. M., Dunkley J., Bennett C. L., Gold B., Hinshaw G., Jarosik N., Larson D., et al. 2011, *ApJS*, 192, 18
- Lacey C., Cole S., 1993, *MNRAS*, 262, 627
- Lacey C. G., Baugh C. M., Frenk C. S., Benson A. J., 2011, *MNRAS*, 412, 1828
- Mac Low M.-M., McCray R., 1988, *ApJ*, 324, 776
- McLure R. J., Cirasuolo M., Dunlop J. S., Foucaud S., Almaini O., 2009, *MNRAS*, 395, 2196
- McQuinn M., Lidz A., Zahn O., Dutta S., Hernquist L., Zaldarriaga M., 2007, *MNRAS*, 377, 1043
- Mesinger A., Dijkstra M., 2008, *MNRAS*, 390, 1071
- Meurer G. R., Heckman T. M., Calzetti D., 1999, *ApJ*, 521, 64
- Miralda-Escudé J., Haehnelt M., Rees M. J., 2000, *ApJ*, 530, 1
- Mo H. J., Mao S., White S. D. M., 1998, *MNRAS*, 295, 319
- Muñoz J. A., Loeb A., 2011, *ApJ*, 729, 99
- Oey M. S., Clarke C. J., 1997, *MNRAS*, 289, 570
- Oh S. P., Furlanetto S. R., 2005, *ApJL*, 620, L9

² An important caveat to this conclusion is the possibility of a top-heavy mass function of Population-III stars in small galaxies, since in this case the ionizing efficiency is much larger than for Population-II stars, so that low-mass galaxies could make a more important contribution to reionization in this case.

- Press W. H., Schechter P., 1974, *ApJ*, 187, 425
- Raičević M., Theuns T., Lacey C., 2011, *MNRAS*, 410, 775
- Razoumov A. O., Sommer-Larsen J., 2006, *ApJL*, 651, L89
- Rocha M., Peter A. H. G., Bullock J., 2012, *MNRAS*, p. 3471
- Salvaterra R., Ferrara A., Dayal P., 2011, *MNRAS*, 414, 847
- Scalo J., 1998, in Gilmore G., Howell D., eds, *The Stellar Initial Mass Function (38th Herstmonceux Conference)* Vol. 142 of *Astronomical Society of the Pacific Conference Series*, *The IMF Revisited: A Case for Variations*. p. 201
- Shapley A. E., Steidel C. C., Pettini M., Adelberger K. L., Erb D. K., 2006, *ApJ*, 651, 688
- Sheth R. K., Tormen G., 1999, *MNRAS*, 308, 119
- Siana B., Teplitz H. I., Colbert J., Ferguson H. C., Dickinson M., Brown T. M., Conselice C. J., de Mello D. F., Gardner J. P., Giavalisco M., Menanteau F., 2007, *ApJ*, 668, 62
- Smit R., Bouwens R. J., Franx M., Illingworth G. D., Labbé I., Oesch P. A., van Dokkum P. G., 2012, *ArXiv e-prints*
- Srbnovsky J. A., Wyithe J. S. B., 2007, *MNRAS*, 374, 627
- Steidel C. C., Pettini M., Adelberger K. L., 2001, *ApJ*, 546, 665
- Storrie-Lombardi L. J., McMahon R. G., Irwin M. J., Hazard C., 1994, *ApJL*, 427, L13
- Thoul A. A., Weinberg D. H., 1996, *ApJ*, 465, 608
- Trenti M., Stiavelli M., Bouwens R. J., Oesch P., Shull J. M., Illingworth G. D., Bradley L. D., Carollo C. M., 2010, *ApJL*, 714, L202
- Wise J. H., Cen R., 2009, *ApJ*, 693, 984
- Wood K., Loeb A., 2000, *ApJ*, 545, 86
- Wyithe J. S. B., Bolton J. S., 2011, *MNRAS*, 412, 1926
- Wyithe J. S. B., Bolton J. S., Haehnelt M. G., 2008, *MNRAS*, 383, 691
- Wyithe J. S. B., Loeb A., 2003a, *ApJ*, 586, 693
- Wyithe J. S. B., Loeb A., 2003b, *ApJ*, 595, 614
- Wyithe J. S. B., Loeb A., 2011, *MNRAS*, 413, L38
- Yajima H., Umemura M., Mori M., Nakamoto T., 2009, *MNRAS*, pp 1070–+
- Zahn O., Reichardt C. L., Shaw L., Lidz A., Aird K. A., Benson B. A., Bleem L. E., Carlstrom J. E., et al. 2012, *ApJ*, 756, 65